Treatment of discontinuity in the reproducing kernel element method

Hongsheng Lu[1], Do Wan Kim[2,‡] and Wing Kam Liu[1,*,†]

[1]*Department of Mechanical Engineering, Northwestern University, 2145 Sheridan Road, Evanston, IL 60208-3111, U.S.A.*
[2]*Department of Mathematics, Sunmoon University, 336-708, Asan-si, Choong-nam, Republic of Korea*

SUMMARY

A discontinuous reproducing kernel element approximation is proposed in the case where weak discontinuity exists over an interface in the physical domain. The proposed method can effectively take care of the discontinuity of the derivative by truncating the window function and global partition polynomials. This new approximation keeps the advantage of both finite element methods and meshfree methods as in the reproducing kernel element method. The approximation has the interpolation property if the support of the window function is contained in the union of the elements associated with the corresponding node; therefore, the continuity of the primitive variables at nodes on the interface is ensured. Furthermore, it is smooth on each subregion (or each material) separated by the interface. The major advantage of the method is its simplicity in implementation and it is computationally efficient compared to other methods treating discontinuity. The convergence of the numerical solution is validated through calculations of some material discontinuity problems. Copyright © 2005 John Wiley & Sons, Ltd.

KEY WORDS: discontinuous reproducing kernel element approximation; interface; weak discontinuity

1. INTRODUCTION

A new class of methods such as the reproducing kernel element method (RKEM) [1–3] and the moving particle finite element method (MPFEM) [4, 5] have been recently developed. The methods in this class have the virtues of both finite element and meshfree approximations [6–9].

In the RKEM, the continuous global partition polynomials constructed from each element are patched over the whole domain [1–3]. For the localization of the global partition polynomials, we adopt the reproducing kernel function such that the subsequent RKE shape function satisfies the reproducing condition for the polynomials and possesses the interpolation property. By doing so, the regularity of the RKE shape function is only determined by the kernel function. As reported in Reference [2], the reproducing kernel element shape function has the Kronecker delta property under certain restrictions on the support size of the kernel function. This interpolation property can play an important role in enforcing the Dirichlet boundary condition in RKEM, which is one of the good properties in a finite element approximation. For the convergence of the numerical solution in the finite element method, Babuška has proven the convergence rate of $h^{1/2}$ in the Sobolev space W_2^1 in the case when the interface does not fit with the elements [10].

The regular meshfree method has to pay some cost to represent accurately discontinuous derivatives on an interface. Several methods have been developed to enrich the meshfree approximation by adding particular functions that contain discontinuities in the derivatives [11–13] or by introducing jump conditions in the variational equations [14]. In References [15, 16], weak discontinuities across an arbitrary interface are treated using the extended finite element method (XFEM) satisfying partitions of unity. In this paper, we develop a new approximation function with derivative discontinuity across the interface based on RKEM. The approximation is said to be the discontinuous reproducing kernel element (DRKE) approximation and it is achieved by cutting off the support of window function along the interface and the global partition polynomials. Consequently, this yields the new partitions of unity affected by the interface. The advantage of RKEM is maintained in the DRKE method. The proposed approximation method can be easily implemented and it can be applied to arbitrary material interfaces.

The outline of the paper is as follows: in Section 2 the RKEM is revisited. Section 3 describes the DRKE approximation and its salient features are characterized. Numerical results are shown in Section 4 to validate the reliability of the method. Conclusions for the method are written in Section 5.

2. REVIEW OF RKEM

Let $\Omega \subset \mathbb{R}^d$ ($d = 1, 2, 3$) be an open, bounded Lipschitz domain with its boundary $\partial\Omega$. With a set S, the symbols $\bar{S}$ and $\mathring{S}$ represent the closure and the interior of the set S, respectively. The open r-ball in $\mathbb{R}^d$ is denoted by $B_r(\mathbf{x})$ when its centre is located at $\mathbf{x}$ and the radius is r.

The closure of domain Ω, $\bar{\Omega}$ is decomposed into a set of closed subdomains $\{\Omega_n\}_{n=1}^N$, which satisfy the following conditions:

1. each Ω_n is a closed set with non-empty interior,
2. $\bar{\Omega} = \bigcup_{n=1}^N \Omega_n$,
3. $\mathring{\Omega}_i \cap \mathring{\Omega}_j = \emptyset$ for $i \neq j$.

On each subdomain Ω_n, we assume that there exists a linearly independent set of global partition polynomials $\{\psi_{n,i}(\mathbf{x})\}_{i=1}^{I_n}$ for some integer $I_n \geqslant 1$ and its corresponding nodes $\{\mathbf{x}_{n,i}\}_{i=1}^{I_n}$

such that the following reproducing property of order k holds:

$$\sum_{i=1}^{I_n} \psi_{n,i}(\mathbf{x}) \, \mathbf{x}_{n,i}^{\beta} = \mathbf{x}^{\beta}, \quad \mathbf{x} \in \bar{\Omega}, \ \ |\beta| \leqslant k \tag{1}$$

In the RKEM, we note the continuous global partition polynomial is patched over the whole domain and the compact reproducing kernel function is used to localize the global partition polynomial such that the required reproducing conditions are satisfied. The (quasi-)interpolation of a continuous function is proposed in Reference [2] as follows:

$$\left(\mathcal{I}^{\Omega} v\right)(\mathbf{x}) \equiv \sum_{n=1}^{N} \left[\int_{\Omega_n} K_{\rho}(\mathbf{y} - \mathbf{x}; \mathbf{x}) \, \mathrm{d}\mathbf{y} \sum_{i=1}^{I_n} \psi_{n,i}(\mathbf{x}) v\left(\mathbf{x}_{n,i}\right) \right] = \sum_{I=1}^{NP} \Psi_I(\mathbf{x}) v\left(\mathbf{x}_I\right) \tag{2}$$

where $K_{\rho}(\mathbf{z}; \mathbf{x})$ is a reproducing kernel function whose support is compact with respect to the variable $\mathbf{z}$ and it is usually taken to be equal to $\overline{B_{\rho}(\mathbf{0})}$. NP is the number of nodes on $\bar{\Omega}$ and we have called $\Psi_I(\mathbf{x})$ defined in (2) the reproducing kernel element shape function at node $\mathbf{x}_I$. From now on, the minimum size of subdomains(or mesh) and the support size of window function are denoted by h and ρ, respectively.

In this paper, the following function is adopted as a kernel function:

$$K_{\rho}(\mathbf{y} - \mathbf{x}; \mathbf{x}) = \frac{1}{\rho^d} \, \phi\left(\frac{\mathbf{y} - \mathbf{x}}{\rho}\right) b(\mathbf{x}) \tag{3}$$

where the function $\phi(\mathbf{x})$ is a continuous and non-negative window function with unit support size. The $b(\mathbf{x})$ function can be determined under the condition that $\mathcal{I}^{\Omega} 1 = 1$, which is equivalent to the 0th reproducing condition. Hence, if $S - \mathbf{x}/\rho$ for a set S denotes the $\mathbf{x}$-translated and ρ-dilated set defined as

$$\frac{S - \mathbf{x}}{\rho} \equiv \left\{ \frac{\mathbf{y} - \mathbf{x}}{\rho} \,\middle|\, \mathbf{y} \in S \right\} \tag{4}$$

then the correct kernel function in this case has the following form:

$$K_{\rho}(\mathbf{y} - \mathbf{x}; \mathbf{x}) = \frac{1}{\rho^d} \, \frac{\phi(\mathbf{y} - \mathbf{x}/\rho)}{\int_{(\Omega - \mathbf{x}/\rho) \cap B_1(\mathbf{0})} \phi(\mathbf{z}) \, \mathrm{d}\mathbf{z}} \tag{5}$$

If we define partitions of unity $\{\lambda_n(\mathbf{x})\}_{n=1}^{N}$ such that

$$\lambda_n(\mathbf{x}) \equiv \frac{\int_{(\Omega_n - \mathbf{x}/\rho) \cap B_1(\mathbf{0})} \phi(\mathbf{z}) \, \mathrm{d}\mathbf{z}}{\int_{(\Omega - \mathbf{x}/\rho) \cap B_1(\mathbf{0})} \phi(\mathbf{z}) \, \mathrm{d}\mathbf{z}} \tag{6}$$

then the approximation formula can be rewritten as follows [17]:

$$\left(\mathcal{I}^{\Omega} v\right)(\mathbf{x}) = \sum_{n=1}^{N} \left[\lambda_n(\mathbf{x}) \sum_{i=1}^{I_n} \psi_{n,i}(\mathbf{x}) v\left(\mathbf{x}_{n,i}\right) \right] \tag{7}$$
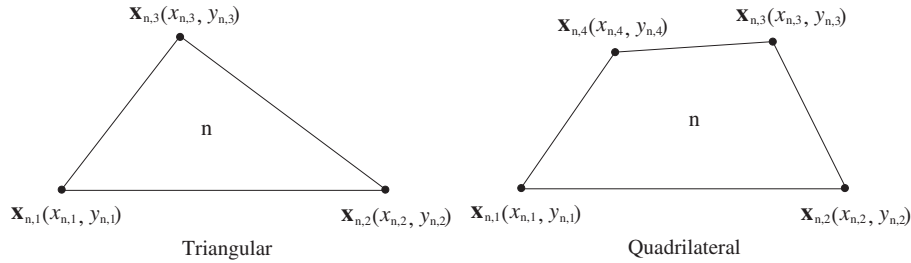
Figure 1. Typical 2-D subdomain Ω_n.

The salient features of the operator $\mathcal{I}^{\Omega}$ defined in (2) are addressed in Reference [2] such that

- The operator reproduces the global partition polynomials if and only if it preserves the unit function, i.e. $\mathcal{I}^{\Omega} 1 = 1$.
- The regularity of the shape function $\Psi_I(\mathbf{x})$ is determined by the kernel function.
- Under the hypothesis that all shape functions are linearly independent in Ω, we have $\Psi_I(\mathbf{x}_J) = \delta_{IJ}$ or $(\mathcal{I}^{\Omega} v)(\mathbf{x}_I) = v(\mathbf{x}_I)$ for a node $\mathbf{x}_I$, provided the support of the kernel function in the first argument is contained in the union of all adjacent elements at $\mathbf{x}_I$.

The systematic procedure to construct the global partition polynomial is given in References [1, 3]. If a triangular element shown in Figure 1 is chosen as a subdomain, then the global partition polynomials with the linear reproducing property can be constructed from (1) as follows:

$$
\begin{bmatrix} \psi_{n,1}(\mathbf{x}) \\ \psi_{n,2}(\mathbf{x}) \\ \psi_{n,3}(\mathbf{x}) \end{bmatrix} = \begin{bmatrix} (\mathbf{x} - \mathbf{x}_{n,1})^{(0,0)} & (\mathbf{x} - \mathbf{x}_{n,2})^{(0,0)} & (\mathbf{x} - \mathbf{x}_{n,3})^{(0,0)} \\ (\mathbf{x} - \mathbf{x}_{n,1})^{(1,0)} & (\mathbf{x} - \mathbf{x}_{n,2})^{(1,0)} & (\mathbf{x} - \mathbf{x}_{n,3})^{(1,0)} \\ (\mathbf{x} - \mathbf{x}_{n,1})^{(0,1)} & (\mathbf{x} - \mathbf{x}_{n,2})^{(0,1)} & (\mathbf{x} - \mathbf{x}_{n,3})^{(0,1)} \end{bmatrix}^{-1} \begin{bmatrix} 1 \\ 0 \\ 0 \end{bmatrix} \tag{8}
$$

where we use the multi-index notations such that

$$
\mathbf{z}^{\beta} \equiv z_1^{\beta_1} z_2^{\beta_2} \quad \text{when } \mathbf{z} = (z_1, z_2) \in \mathbb{R}^2, \beta = (\beta_1, \beta_2) \in \mathbb{N}^2 \tag{9}
$$

and hence $(\mathbf{x} - \mathbf{x}_{n,i})^{\beta}$ for $\beta = (0,0)$, $(1,0)$, and $(0,1)$ is scalar. The global partition polynomial exists as long as the area of the triangular subdomain is non-zero. It can be shown that the global partition polynomials are identical to the finite element shape function inside the subdomain/element for this case. Similarly, the global partition polynomials for a bilinear
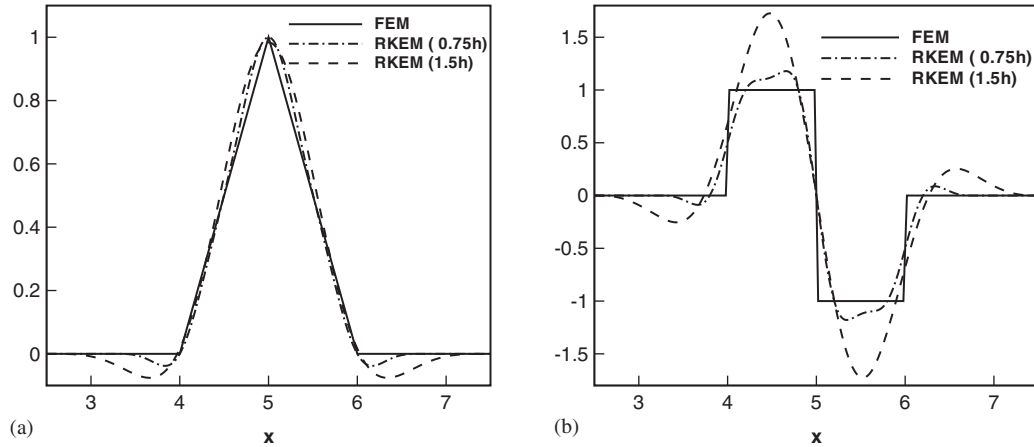
Figure 2. Comparison of shape function and its derivative in FEM and RKEM ($\rho = 0.75\,h, 1.5\,h$): (a) shape functions; and (b) derivative of shape functions.

quadrilateral element as illustrated in Figure 1 can be shown to be

$$
\begin{bmatrix}
\psi_{n,1}(\mathbf{x}) \\
\psi_{n,2}(\mathbf{x}) \\
\psi_{n,3}(\mathbf{x}) \\
\psi_{n,4}(\mathbf{x})
\end{bmatrix}
=
\begin{bmatrix}
(\mathbf{x} - \mathbf{x}_{n,1})^{(0,0)} & (\mathbf{x} - \mathbf{x}_{n,2})^{(0,0)} & (\mathbf{x} - \mathbf{x}_{n,3})^{(0,0)} & (\mathbf{x} - \mathbf{x}_{n,4})^{(0,0)} \\
(\mathbf{x} - \mathbf{x}_{n,1})^{(1,0)} & (\mathbf{x} - \mathbf{x}_{n,2})^{(1,0)} & (\mathbf{x} - \mathbf{x}_{n,3})^{(1,0)} & (\mathbf{x} - \mathbf{x}_{n,4})^{(1,0)} \\
(\mathbf{x} - \mathbf{x}_{n,1})^{(0,1)} & (\mathbf{x} - \mathbf{x}_{n,2})^{(0,1)} & (\mathbf{x} - \mathbf{x}_{n,3})^{(0,1)} & (\mathbf{x} - \mathbf{x}_{n,4})^{(0,1)} \\
(\mathbf{x} - \mathbf{x}_{n,1})^{(1,1)} & (\mathbf{x} - \mathbf{x}_{n,2})^{(1,1)} & (\mathbf{x} - \mathbf{x}_{n,3})^{(1,1)} & (\mathbf{x} - \mathbf{x}_{n,4})^{(1,1)}
\end{bmatrix}^{-1}
\begin{bmatrix}
1 \\
0 \\
0 \\
0
\end{bmatrix}
\tag{10}
$$

where the term $(\mathbf{x} - \mathbf{x}_{n,i})^{(1,1)}$ produces the bilinear global partition polynomial since we have $(\mathbf{x} - \mathbf{x}_{n,i})^{(1,1)} = (x - x_{n,i})(y - y_{n,i})$ for each $i = 1, \ldots, 4$ in $\mathbb{R}^2$.

The comparison of the reproducing kernel element shape function to the corresponding finite element shape function is depicted in Figure 2 for a 1-D linear uniform element together with their corresponding derivative. Figure 2 clearly shows the unique properties of RKEM, i.e. the presence of Kronecker delta condition and the high regularity of the shape function, which depends on that of the window function.

3. TREATMENT OF DISCONTINUITY

The smooth approximation in meshfree methods leads to difficulties in representing derivative discontinuities along an interface. Several methods have been proposed to enrich the meshfree approximation by adding special functions that contain discontinuities in the derivatives [12–14]. However, by defining new partitions of unity due to restricting the window function on each

subregion, we can achieve the approximation which has the derivative discontinuity along the interface.

Let $\chi_S(\mathbf{x})$ be the characteristic function of $\bar{S}$ if S is a set in $\mathbb{R}^d$. For simplicity, assume the interface Γ divides the considered domain Ω into two open subregions of Ω_A and Ω_B. As a matter of fact, the subsequent procedure does not depend on the number of subregions. Assuming the class of subdomains $\{\Omega_n\}_{n=1}^N$ is made from the interface fitted triangulation so that the interface is located at some edges of Ω_n's, we consider the following approximation modified from the interpolation (7):

$$\left(\mathcal{I}^\Gamma v\right)(\mathbf{x}) = \sum_{n=1}^N \left[\lambda_n^\Gamma(\mathbf{x}) \sum_{i=1}^{I_n} \psi_{n,i}(\mathbf{x}) v\left(\mathbf{x}_{n,i}\right) \right] \equiv \sum_{I=1}^{NP} \Psi_I^\Gamma(\mathbf{x}) v\left(\mathbf{x}_I\right) \tag{11}$$

where $\{\lambda_n^\Gamma\}_{n=1}^N$ are modified partitions of unity defined as the following:

$$\lambda_n^\Gamma(\mathbf{x}) \equiv \frac{\left(\int_{((\Omega_n \cap \Omega_A) - \mathbf{x}/\rho) \cap B_1(\mathbf{0})} \phi(\mathbf{z})\,d\mathbf{z}\right) \chi_{\Omega_A}(\mathbf{x}) + \left(\int_{((\Omega_n \cap \Omega_B) - \mathbf{x}/\rho) \cap B_1(\mathbf{0})} \phi(\mathbf{z})\,d\mathbf{z}\right) \chi_{\Omega_B}(\mathbf{x})}{\left(\int_{(\Omega_A - \mathbf{x}/\rho) \cap B_1(\mathbf{0})} \phi(\mathbf{z})\,d\mathbf{z}\right) \chi_{\Omega_A}(\mathbf{x}) + \left(\int_{(\Omega_B - \mathbf{x}/\rho) \cap B_1(\mathbf{0})} \phi(\mathbf{z})\,d\mathbf{z}\right) \chi_{\Omega_B}(\mathbf{x})} \tag{12}$$

The integral regions $\Omega_n \cap \Omega_A$ and $\Omega_n \cap \Omega_B$ in the above equation make the global partition polynomials restricted to Ω_A and Ω_B, respectively, while the role of the characteristic functions $\chi_{\Omega_A}(\mathbf{x})$ and $\chi_{\Omega_B}(\mathbf{x})$ is to divide the whole domain into the subregions Ω_A and Ω_B and produce new partitions of unity on each subregion.

If $v(\mathbf{x})$ is a continuous function on $\bar{\Omega}$, then we can verify that the operator $\mathcal{I}^\Gamma$ has the following features as well:

- We have the following identity

$$\left(\mathcal{I}^\Gamma v\right)(\mathbf{x}) = \begin{cases} \left(\mathcal{I}^{\Omega_A} v|_{\Omega_A}\right)(\mathbf{x})\chi_{\Omega_A}(\mathbf{x}) + \left(\mathcal{I}^{\Omega_B} v|_{\Omega_B}\right)(\mathbf{x})\chi_{\Omega_B}(\mathbf{x}), & \mathbf{x} \notin \Gamma \\ \left(\mathcal{I}^{\Omega_A \cup \Omega_B} v\right)(\mathbf{x}), & \mathbf{x} \in \Gamma \end{cases} \tag{13}$$

- At every point $\mathbf{x} \in \Gamma$ that is not a node, we have in general

$$\lim_{\mathring{\Omega}_A \ni \mathbf{y} \to \mathbf{x}} \left(\mathcal{I}^\Gamma v\right)(\mathbf{y}) \neq \lim_{\mathring{\Omega}_B \ni \mathbf{y} \to \mathbf{x}} \left(\mathcal{I}^\Gamma v\right)(\mathbf{y}) \tag{14}$$

  However, if $\mathbf{x}_I$ is a node on Γ, then $\left(\mathcal{I}^\Gamma v\right)(\mathbf{x})$ is continuous at $\mathbf{x}_I$ whenever the support of the kernel function at $\mathbf{x}_I$ is contained in the union of all adjacent elements touching the support.

- The limit of $D_\mathbf{x}^\beta \left(\mathcal{I}^\Gamma v\right)(\mathbf{x})(|\beta| = 1)$ exists as the point $\mathbf{x}$ on each side of the interface approaches a point on Γ. Furthermore, the approximation by the operator $\mathcal{I}^\Gamma$ obviously has a discontinuity of its derivative across the interface, which is our desired property.

- If the characteristic functions $\{\chi_{\Omega_n}(\mathbf{x})\}$ take the place of $\{\Omega_A, \Omega_B\}$, then this method reduces to FEM.

We will call the approximation operator $\mathcal{I}^\Gamma$ the *DRKE operator on* Γ and also $\left\{\Psi_I^\Gamma(\mathbf{x})\right\}_{n=1}^{NP}$ will be called *the DRKE shape functions*. As shown in Figure 3, the interface is defined by the common nodes belonging to the adjacent materials. The continuity of solution at the
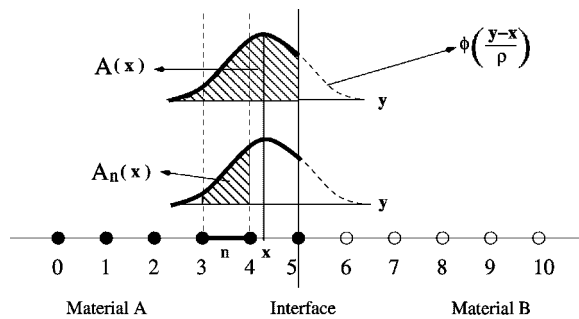
Figure 3. The concept of DRKE for 1-D case: the new partition of unity $\lambda_n^\Gamma(\mathbf{x}) = A_n(\mathbf{x})/A(\mathbf{x})$.
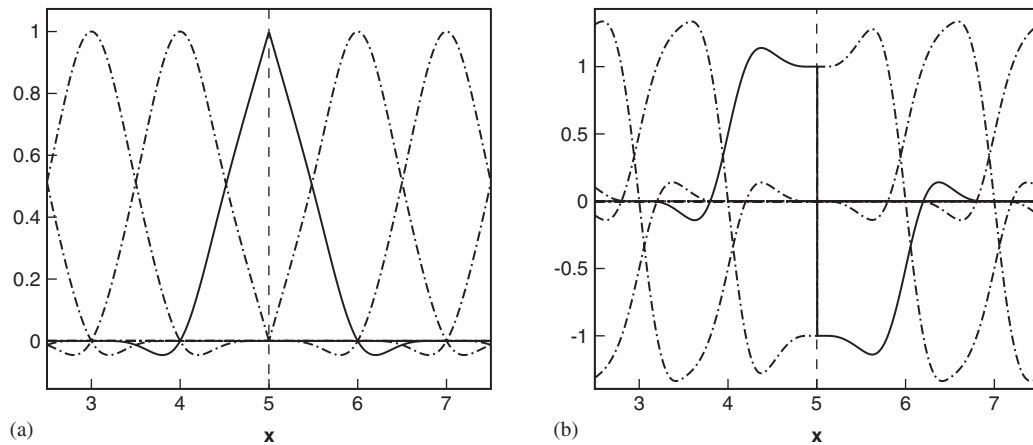

Figure 4. 1-D Shape functions and their derivatives near the interface ($x = 5$): (a) DRKE shape functions; and (b) derivative of DRKE shape function.

common nodes on the interface is satisfied due to the interpolation property of reproducing kernel element shape function. Although there is a solution discrepancy for points between two nodes, the convergence of interpolation on each subregion makes the discrepancy decrease as the discretization along the interface becomes fine.

To figure out the scheme to treat discontinuity, first we consider the case of a 1-D interface problem as shown in Figure 3. The nodes numbered from 0 to 5 belong to material A, and the nodes numbered from 5 to 10 belong to material B. The common node 5 on the interface belongs to both materials A and B. The DRKE shape function and its derivative are also shown in Figure 4 under the situation of derivative discontinuity at the common node 5.

On the other hand, to calculate the derivative of shape functions in the discrete reproducing kernel element approximation, we need the following derivative formula for the integral of compactly supported and continuous function in $\mathbb{R}^d$ over the translating domain $S(\mathbf{x}) \equiv S_0 - \mathbf{x}$

for $\mathbf{x} \in \mathbb{R}^d$, i.e. if $\phi(\mathbf{z}) \in C^0\left(\mathbb{R}^d\right)$ and supp $\phi \subset B_1(\mathbf{0})$, then we have

$$D_{\mathbf{x}}^{\beta}\left(\int_{S(\mathbf{x}) \cap B_1(\mathbf{0})} \phi(\mathbf{z}) \, \mathrm{d}\mathbf{z}\right) = \int_{\partial S(\mathbf{x}) \cap B_1(\mathbf{0})} (\beta \cdot \mathbf{n}) \phi(\mathbf{z}) \, \mathrm{d}\gamma, \quad |\beta| = 1 \tag{15}$$

where $\mathrm{d}\gamma$ represents the length(or surface) Lebesque measure. It suffices to derive the first-order derivatives of the modified partition of unity $\lambda_n^{\Gamma}(\mathbf{x})$ for each nth subdomain in (12) in order to calculate $D^{\beta}\mathcal{I}^{\Gamma}v(\mathbf{x})$ for $|\beta| = 1$. Therefore, from formula (15), we have the following derivatives for any $\mathbf{x} \in \Omega \backslash \Gamma$:

$$D^{\beta}\lambda_n^{\Gamma}(\mathbf{x}) = \frac{1}{\rho}\left[\frac{V_n^{\partial A}(\mathbf{x})\chi_{\Omega_A}(\mathbf{x}) + V_n^{\partial B}(\mathbf{x})\chi_{\Omega_B}(\mathbf{x})}{V^A(\mathbf{x})\chi_{\Omega_A}(\mathbf{x}) + V^B(\mathbf{x})\chi_{\Omega_B}(\mathbf{x})} - \frac{V_n^A(\mathbf{x})V^{\partial A}(\mathbf{x})\chi_{\Omega_A}(\mathbf{x}) + V_n^B(\mathbf{x})V^{\partial B}(\mathbf{x})\chi_{\Omega_B}(\mathbf{x})}{V^A(\mathbf{x})^2\chi_{\Omega_A}(\mathbf{x}) + V^B(\mathbf{x})^2\chi_{\Omega_B}(\mathbf{x})}\right]$$

$$\tag{16}$$

where the functions appearing in the above equation are defined as follows:

$$V^A(\mathbf{x}) \equiv \int_{(\Omega_A - \mathbf{x}/\rho) \cap B_1(\mathbf{0})} \phi(\mathbf{z}) \, \mathrm{d}\mathbf{z}$$

$$V^B(\mathbf{x}) \equiv \int_{(\Omega_B - \mathbf{x}/\rho) \cap B_1(\mathbf{0})} \phi(\mathbf{z}) \, \mathrm{d}\mathbf{z}$$

$$V_n^A(\mathbf{x}) \equiv \int_{((\Omega_n \cap \Omega_A) - \mathbf{x}/\rho) \cap B_1(\mathbf{0})} \phi(\mathbf{z}) \, \mathrm{d}\mathbf{z}$$

$$V_n^B(\mathbf{x}) \equiv \int_{((\Omega_n \cap \Omega_B) - \mathbf{x}/\rho) \cap B_1(\mathbf{0})} \phi(\mathbf{z}) \, \mathrm{d}\mathbf{z}$$

$$V^{\partial A}(\mathbf{x}) \equiv \int_{\partial(\Omega_A - \mathbf{x}/\rho) \cap B_1(\mathbf{0})} (\beta \cdot \mathbf{n}) \phi(\mathbf{z}) \, \mathrm{d}\gamma$$

$$V^{\partial B}(\mathbf{x}) \equiv \int_{\partial(\Omega_B - \mathbf{x}/\rho) \cap B_1(\mathbf{0})} (\beta \cdot \mathbf{n}) \phi(\mathbf{z}) \, \mathrm{d}\gamma$$

$$V_n^{\partial A}(\mathbf{x}) \equiv \int_{\partial((\Omega_n \cap \Omega_A) - \mathbf{x}/\rho) \cap B_1(\mathbf{0})} (\beta \cdot \mathbf{n}) \phi(\mathbf{z}) \, \mathrm{d}\gamma$$

$$V_n^{\partial B}(\mathbf{x}) \equiv \int_{\partial((\Omega_n \cap \Omega_B) - \mathbf{x}/\rho) \cap B_1(\mathbf{0})} (\beta \cdot \mathbf{n}) \phi(\mathbf{z}) \, \mathrm{d}\gamma$$

where the symbol $\partial(\cdot)$ means the boundary of the domain in $(\cdot)$. Since a Galerkin method is adopted to solve the elastic problems with derivative discontinuities, the calculations of the first-order derivatives are enough.

A two-dimensional domain composed of contacting two materials A and B is discretized with a triangular mesh as shown in Figure 5. The RKE and the DRKE shape function in the radial direction passing through the node $\mathbf{x}_I$ and the interfacial direction from the node $\mathbf{x}_I$ to the
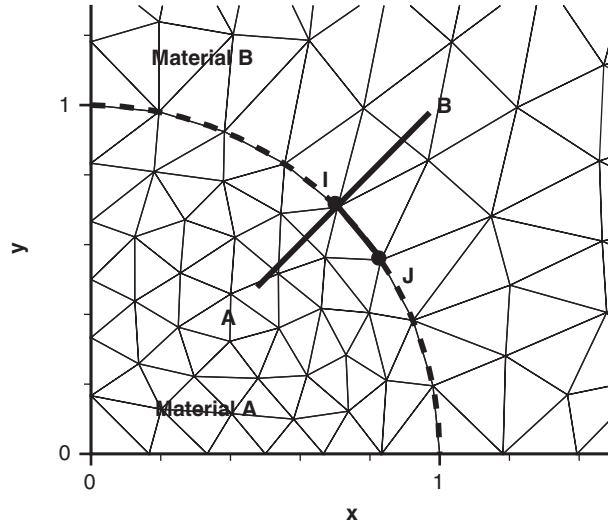
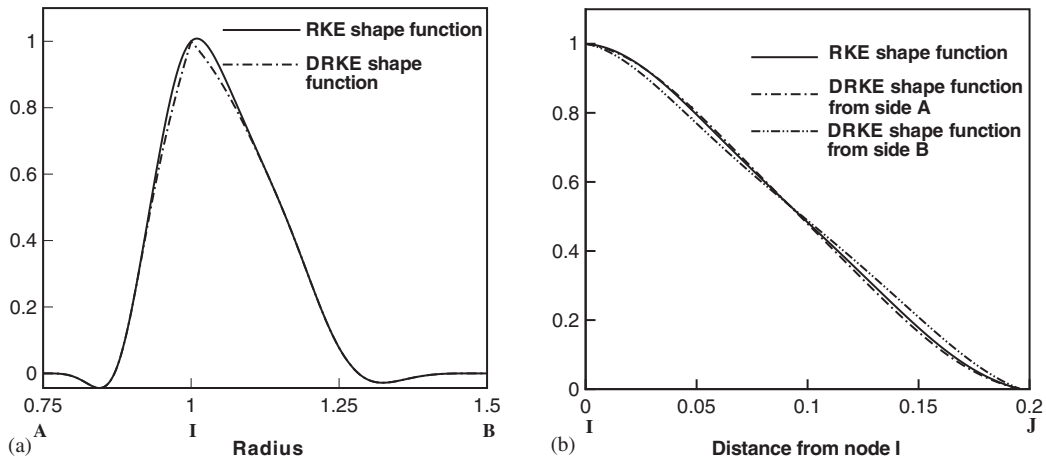Figure 5. Triangulation along the interface in 2-D.

Figure 6. Sectional view of DRKE shape function $\Psi_I^\Gamma(\mathbf{x})$ in 2-D: (a) radial section through $\mathbf{x}_I$; and (b) interfacial section from $\mathbf{x}_I$ to $\mathbf{x}_J$.

node $\mathbf{x}_J$ about the interface are depicted in Figure 6, respectively. As we anticipated, although the deviations of the DRKE shape function values across the interface take place between nodes, the shape function has the continuity property at all nodes on the interface since it has the Kronecker delta property. On each material domain, we have proved the convergence for the RKE interpolation (see Reference [2]) and, from the property (13) of the operator $\mathcal{I}^\Gamma$, the difference value of the shape function approaches zero as the mesh size h goes to zero.

The radial section view of derivatives of the DRKE shape function passing across $\mathbf{x}_I$ is shown in Figure 7. To clarify the derivative jumps of DRKE shape function on the interface,
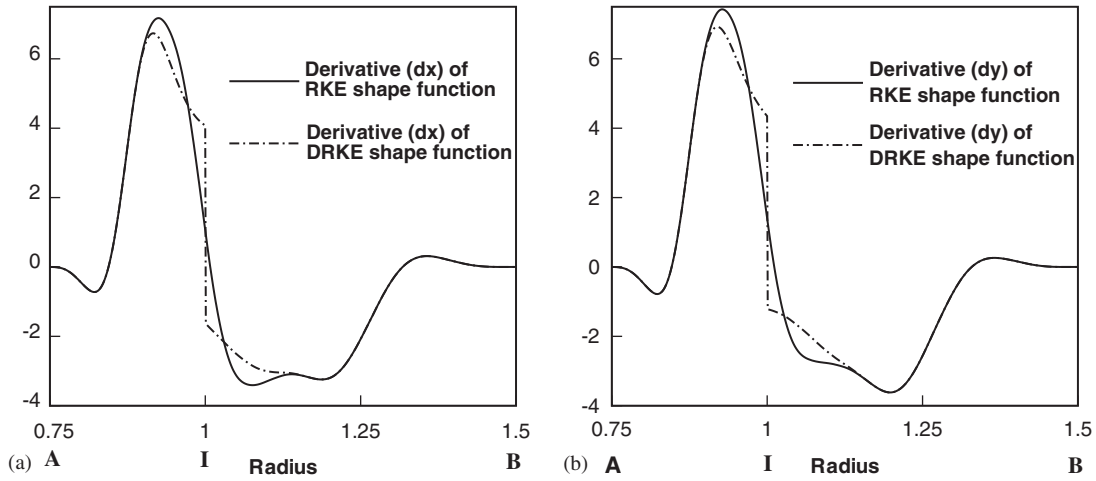
Figure 7. Derivatives of shape function $\Psi_I^\Gamma(\mathbf{x})$ on the radial section passing through node $\mathbf{x}_I$: (a) $D^{(1,0)}\Psi_I^\Gamma(\mathbf{x})$; and (b) $D^{(0,1)}\Psi_I^\Gamma(\mathbf{x})$.
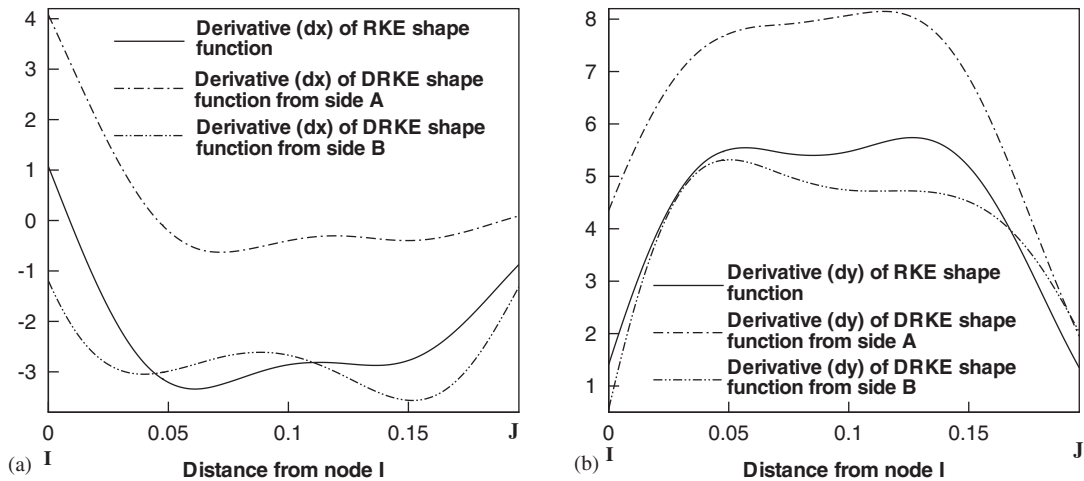

Figure 8. Derivatives of shape function $\Psi_I^\Gamma(\mathbf{x})$ on the interfacial section from $\mathbf{x}_I$ to $\mathbf{x}_J$: (a) $D^{(1,0)}\Psi_I^\Gamma(\mathbf{x})$; and (b) $D^{(0,1)}\Psi_I^\Gamma(\mathbf{x})$.

Figure 8 shows the interfacial section view of the derivative of DRKE shape functions. In the figure, the derivative jump of the shape function is clearly seen on the interface. In general, the derivative values of DRKE shape function on both sides of the interface are different from each other as can be seen in the figure.
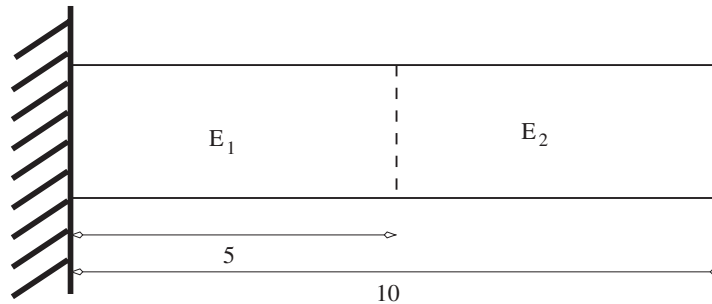
Figure 9. One-dimensional bi-material rod.

4. NUMERICAL EXAMPLES

4.1. One-dimensional bi-material rod

A one-dimensional elastic bi-material rod as shown in Figure 9 is subjected to body force $b(x) = x$. The elastic moduli of the two materials are taken such that $E_1 = 1$ and $E_2 = 0.5$, respectively. Then, this problem has the solution with derivative discontinuity at the material interface and the analytic solution of this problem is known to be the following:

$$u(x) = \begin{cases} \dfrac{1}{E_1}\left(CE_2x - \dfrac{x^3}{6}\right), & x < 5 \\ C(x - 10) + \dfrac{1}{6E_2}\left(1000 - x^3\right) + 1, & x \geqslant 5 \end{cases} \tag{17}$$

where $C = (6E_1 \times E_2 + 875\,E_1 + 125\,E_2)/(30\,E_2\,(E_1 + E_2))$.

The problem is solved by using FEM and DRKEM with linear consistency. Let $h > 0$ be the minimum distance among nodes. The convergence rates of numerical solution in displacement and derivative are illustrated in Figures 10(a) and (b) for FEM and DRKEM. The same convergence rate can be observed; however, the solution of DRKEM with support size h is more accurate than that of FEM. A continuous solution in derivative except on the material interface is obtained in DRKEM as shown in Figure 11.

4.2. Inclusion in an infinite plate

The problem of a cylindrical material inclusion with a constant eigenstrain ε^* embedded in an infinite plate as shown in Figure 12 is considered. The exact solution of the displacement for this problem can be shown to be

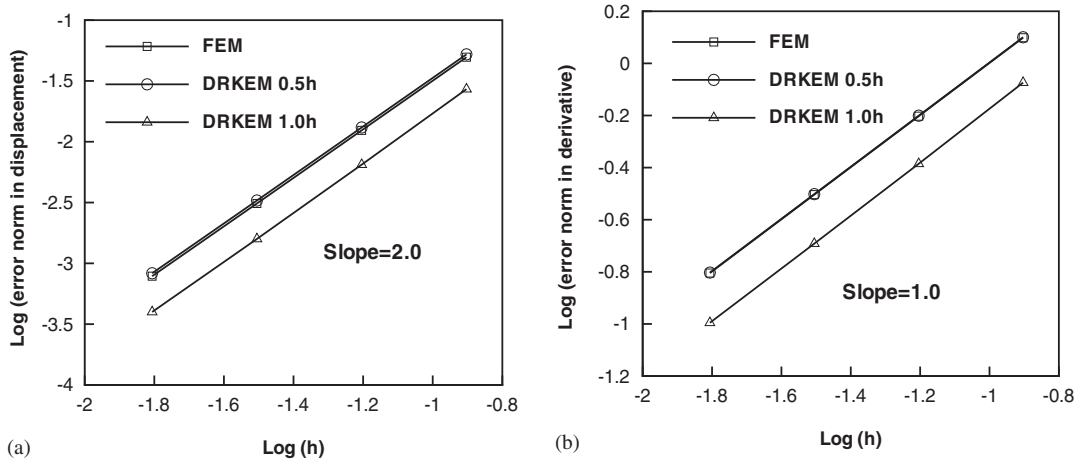$$u_r = \begin{cases} C_1 r, & r < R \\ C_1 \dfrac{R^2}{r}, & r \geqslant R \end{cases} \tag{18}$$

Figure 10. Comparison of convergence rate for the bi-material problem in FEM and DRKEM: (a) convergence rate in primary variable; and (b) convergence rate in the derivative.
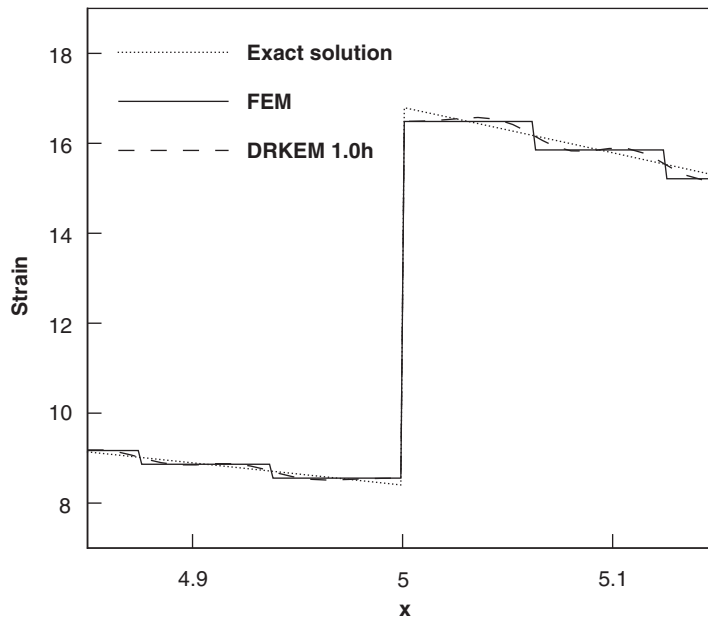

Figure 11. Comparison of strain in FEM and DRKEM.

and the corresponding strain fields are represented as follows:

$$\varepsilon_{rr} = \begin{cases} C_1, & r < R \\ -C_1 \dfrac{R^2}{r^2}, & r \geqslant R \end{cases} \tag{19}$$
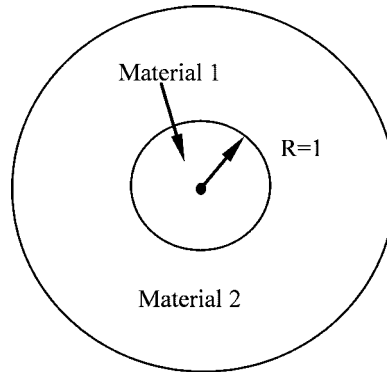
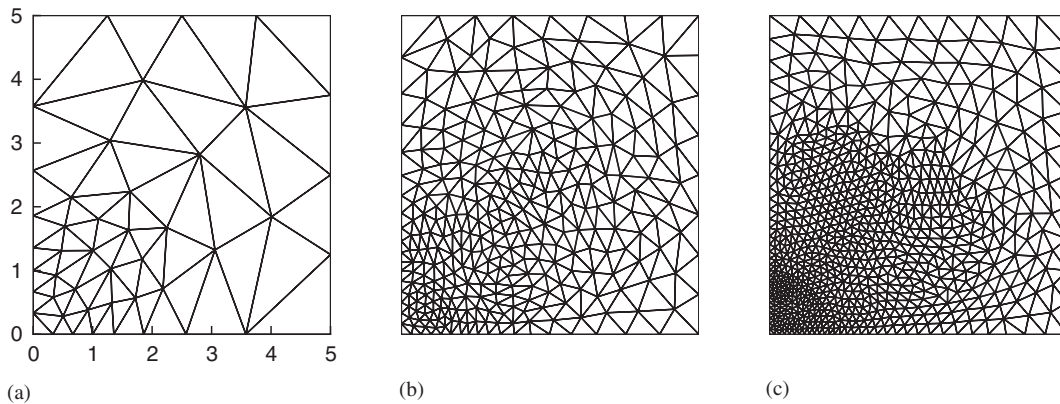Figure 12. Inclusion in an infinite plate.

(a) (b) (c)

Figure 13. Discretizations of the circular inclusion problem: (a) 85 nodes with 5 nodes on the interface; (b) 357 nodes with 9 nodes on the interface; and (c) 1317 nodes with 17 nodes on the interface.

$$
\varepsilon_{\theta\theta} =
\begin{cases}
C_1, & r < R \\
C_1 \dfrac{R^2}{r^2}, & r \geqslant R
\end{cases}
\tag{20}
$$

where $C_1 = \left((\lambda_1 + \mu_1)/(\lambda_1 + \mu_1 + \mu_2) \right) \varepsilon^*$.

For convenience, $R = 1$ is chosen to be the radius of inclusion and μ_i $(i = 1, 2)$ is the Lamé constant for the subdomain Ω_i $(i = 1, 2)$: $\lambda_1 = 497.16$, $\mu_1 = 390.63$ and $\lambda_2 = 656.79$, $\mu_2 = 338.35$ for subregions Ω_1 and Ω_2, respectively. The eigenstrain is set to be 0.01. Due to the symmetry of the problem, the first quadrant of the domain with dimension $[0, 5] \times [0, 5]$ is triangulated with 85, 357 and 1317 nodes as shown in Figure 13. Induced displacement boundary conditions from analytical solution are imposed on the top and right boundaries, and the symmetry conditions on the artificial boundaries, the bottom and the left, are imposed.
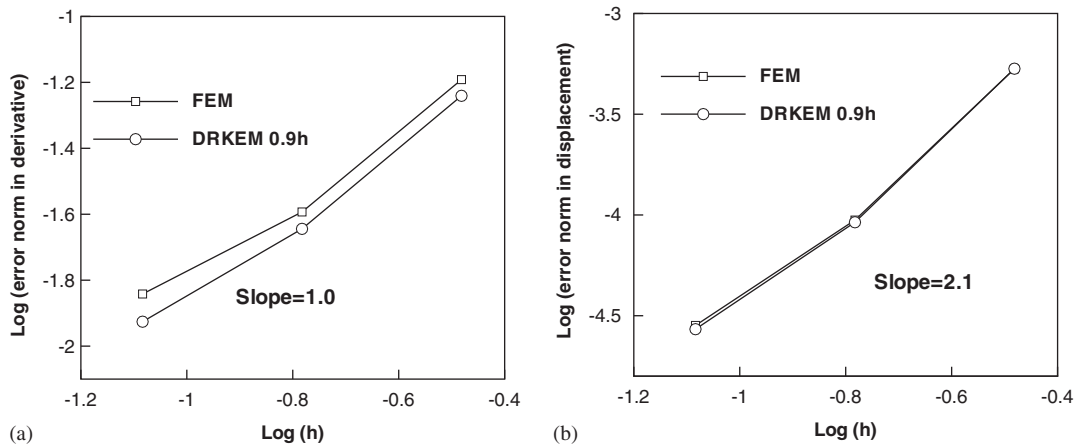
Figure 14. Comparison of convergence rates for the inclusion problem in FEM and DRKEM: (a) convergence rate in primary variable; and (b) convergence rate in the derivative.
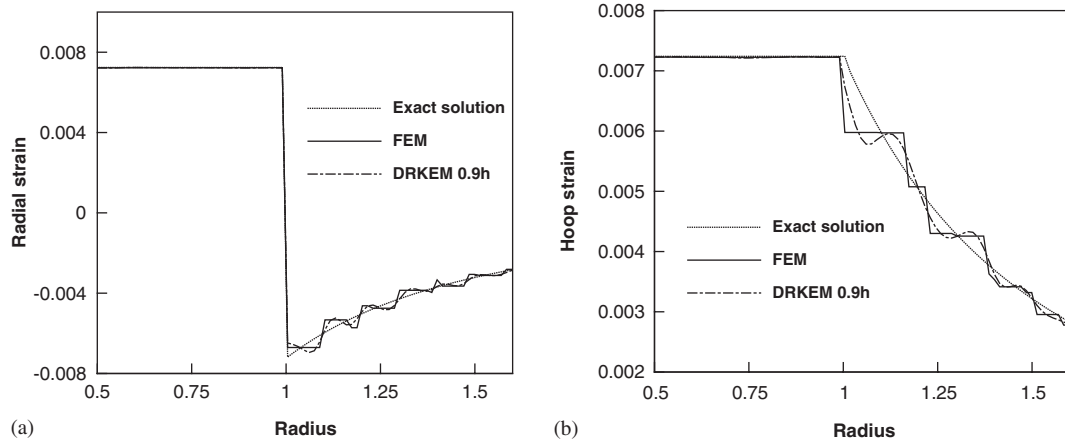

Figure 15. Comparison of strain in FEM and DRKEM: (a) hoop strain; and (b) radial strain.

The numerical example shows that the derivative discontinuity can be effectively treated in DRKEM by controlling the influence domain of the node along the interface. The convergence rate of the numerical solution in the primary variable and in the derivative is shown in Figure 14 for FEM and DRKEM. In this case, the finite element edges coincide with the interface when calculating the numerical solution in FEM. The hoop and radial strains obtained by FEM and DRKEM are compared in Figure 15 for the fine mesh with 1317 nodes.

5. CONCLUSIONS

A new method of treating the discontinuity is proposed in this paper based on the RKEM. By restricting the support of the window function and the subdomains on every subregion

separated by the interface, the global partition polynomials and the partitions of unity are obtained. As a result, we obtain an approximation defined on the whole domain with derivative jump along the interface. The conditions for displacement continuity along the interface are satisfied due to the interpolation property on each subregion. The approximation proposed in this paper is useful particularly in solving problem involving moving interfaces. Moreover, it is naturally conforming. Thus, the re-meshing procedure can be greatly simplified compared to other methods in which the conforming mesh is essential.

ACKNOWLEDGEMENTS

REFERENCES

1. Li S, Lu H, Han W, Liu WK, Simkins DC. Reproducing kernel element method. Part II: globally conforming I^m/C^n hierarchies. *Computer Methods in Applied Mechanics and Engineering* 2004; **193**:953–987.
2. Liu WK, Han W, Lu H, Li S, Cao J. Reproducing kernel element method. Part I: theoretical formulation. *Computer Methods in Applied Mechanics and Engineering* 2004; **193**:933–951.
3. Lu H, Li S, Simkins DC, Liu WK, Cao J. Reproducing kernel element method. Part III: generalized enrichment and applications. *Computer Methods in Applied Mechanics and Engineering* 2004; **193**:989–1011.
4. Hao S, Liu WK. Revisit of moving particle finite element method. *Fifth World Congress on Computational Mechanics*, Vienna, Austria, July 7–12, 2002.
5. Hao S, Liu WK, Belytschko T. Moving particle finite element method with global smoothness. *International Journal for Numerical Methods in Engineering* 2004; **59**:1007–1020.
6. Belytschko T, Lu YY, Gu L. Element-free Galerkin methods. *International Journal for Numerical Methods in Engineering* 1994; **37**:229–256.
7. Liu WK, Jun S, Zhang YF. Reproducing kernel particle methods. *International Journal for Numerical Methods in Fluids* 1995; **20**:1081–1106.
8. Liu WK, Uras RA, Chen Y. Enrichment of the finite element method with the reproducing kernel particle method. *Journal of Applied Mechanics* 1997; **64**:861–870.
9. Li S, Liu WK. Meshfree particle methods and their applications. *Applied Mechanics Review* 2002; **55**(1):1–34.
10. Babuška I. The finite element method for elliptic equations with discontinuous coefficients. *Computing* 1970; **5**:207–213.
11. Chen JS, Han W, You Y, Meng X. A reproducing kernel method with nodal interpolation property. *International Journal for Numerical Methods in Engineering* 2003; **56**:935–960.
12. Chen JS, Kotta V, Lu H, Wang D, Moldovan D, Wolf D. A variational formulation and a double-grid method for meso-scale modeling of stressed grain growth in polycrystalline materials. *Computer Methods in Applied Mechanics and Engineering* 2004; **193**:1277–1303.
13. Krongauz Y, Belytschko T. EFG approximation with discontinuous derivative. *International Journal for Numerical Methods in Engineering* 1998; **41**:1215–1233.
14. Cordes LW, Moran B. Treatment of material discontinuity in the element-free Galerkin method. *Computer Methods in Applied Mechanics and Engineering* 1996; **139**:75–89.
15. Belytschko T, Moës N, Usui S, Sukumar N, Parimi C. Arbitrary discontinuities in finite elements. *International Journal for Numerical Methods in Engineering* 2001; **50**:993–1013.
16. Sukumar N, Chopp DL, Moës N, Belytschko T. Modeling holes and inclusions by level sets in the extended finite-element method. *Computer Methods in Applied Mechanics and Engineering* 2001; **190**(46–47):6183–6200.
17. Han W, Liu WK. Flexible piecewise approximations based on partition of unity. *Advances in Computational Mathematics*, special issue, to appear.